JOURNAL OF Materials CHEMISTRY

Structural transformation of an alumina-supported MnO_2–CuO oxidation catalyst by hydrothermal impact of sub- and supercritical water

Andreas Martin,* Udo Armbruster, Matthias Schneider, Jörg Radnik and Marga-Martina Pohl

Institut für Angewandte Chemie Berlin-Adlershof e.V., Richard-Willstätter-Str. 12, D-12489 Berlin, Germany

Received 3rd September 2001, Accepted 11th December 2001
First published as an Advance Article on the web 29th January 2002

The structural transformation of a MnO_2–CuO-containing catalyst supported on X-ray amorphous Al_2O_3 used in oxidative conversion of ethyl acetate in water under sub-critical (p = 200 bar, T = 633 K) and supercritical reaction conditions (p = 240 bar, T = 673 K) has been studied by X-ray diffractometry (XRD), X-ray photoelectron spectroscopy (XPS) and transmission electron microscopy (TEM). TEM investigations revealed very small primary crystallites of the parent sample (*ca.* 5–20 nm), in contrast to a catalyst specimen exposed to supercritical water for *ca.* 100–200 hours which exhibited large micron-sized crystallites. This crystallisation process is accompanied by a drastic decline in the catalyst BET surface area. XRD studies support this observation: the basic material is nearly X-ray amorphous whereas the used catalyst shows several crystalline phases (*e.g.* Mn_2O_3, Al_2O_3, AlO(OH)). The patterns of spent catalysts taken from the reactor after different running times also gave evidence for the existence of mixed manganese copper oxides. Furthermore, XRD analysis of the used catalysts revealed a reduction of the basic MnO_2 to Mn_3O_4 and Mn_2O_3; this was also clearly proven by XPS analysis. Hydrolysis runs at supercritical water oxidation conditions showed that ethyl acetate is only hydrolysed into ethanol and acetic acid but, in contrast to these non-catalysed runs, the further oxidation of the hydrolysis products to carbon dioxide and water occurs in the presence of the oxidation catalyst. It may be stated that during time-on-stream up to *ca.* 200 h neither activity nor selectivity was found to significantly change, apart from the found structural alterations.

The unique properties of supercritical water (SCW) have been studied extensively during the last decades. Above its critical point (T_c = 647 K, p_c = 221 bar, ρ_c = 0.32 g cm^{-3}) water offers liquid-like densities and gas-like diffusivities. Many other parameters like polarity, dissociation coefficient and heat capacity, are density-dependent as can be seen from kinetic gas theory[1] and, therefore, they can be varied over a wide range.[2] This ''solvent tuning' offers the possibility to use SCW as a tailor-made solvent and also as a reaction partner for many compounds.[3–5] SCW has also been intensively studied as a reaction medium for hydrothermal synthesis of solids.[6] SCW is completely miscible with many gases like oxygen[7] and it is a good solvent for hydrocarbons.[8–10] Hence, oxidation reactions could be carried out in a homogeneous fluid phase, avoiding transport limitations at phase boundaries as well as in porous solid catalysts.

These properties make SCW an excellent reaction medium for oxidative destruction of hazardous organic waste and, since the early 1980's, many papers have been published dealing with such chemistry under supercritical conditions (supercritical water oxidation, SCWO) (*e.g.* ref. 11). The reaction is carried out usually at temperatures from 773–973 K using different oxidants like hydrogen peroxide, oxygen or air.[12] Results were promising, but this technology still has some drawbacks, *e.g.* corrosion, plugging by non-soluble inorganic materials, expensive high-pressure equipment and/or safety risks. Therefore, the use of heterogeneous catalysts might be desirable to lower the reaction temperature, to increase the space velocity of such processes and to reduce processing costs. The number of papers that describe heterogeneously catalysed oxidations—mainly total oxidation—in SCW is still small; the main problem is to find suitable catalyst materials which are stable under the extreme reaction conditions of supercritical water.[13] Most promising systems are transition metal oxides like MnO_2,[14–18] CuO–ZnO_2,[19,20] MnO_2–CeO_2,[21–23] and also some alumina supported systems.[21,24] Very active MnO_2–CuO catalytic systems supported on Al_2O_3 that should withstand the harsh SCW/SCWO conditions are provided by Carus Chemical, Inc., being commercially available and known as Carulite®.[25–27] However, such catalyst compositions may undergo deep structural and chemical alterations during such reaction conditions. Very recently, Yu and Savage reported on the stability and transformations of bulk MnO_2, bulk TiO_2 and CuO on Al_2O_3 in phenol oxidation under SCWO conditions.[14,27] MnO_2 and TiO_2 showed no dissolution but Cu and Al were found in the effluent stream. Deep structural changes accompanied by metal oxide reduction occurred, *i.e.* MnO_2 was transformed into Mn_2O_3, CuO into Cu_2O, Al_2O_3 support into AlO(OH) and anatase into rutile.

Beside these environmentally driven total oxidation reactions, SCW additionally shows increasing possibilities for use as an environmentally benign reaction solvent for heterogeneously catalysed reactions such as hydrogenation, C–C bond formation and partial oxidation as recently reviewed by Savage.[27] In this connection, it is well known that SCW is also a very interesting solvent for inorganic synthesis as mentioned above.[6,28] The dielectric constant dramatically decreases in the vicinity of the critical point, however, the fluid remains sufficiently polar, keeping the most metal oxyanions soluble. A major driving force for investigations of water as a hydrothermal solvent under high pressures is its role in geochemistry. It is well known that the SCW phase is able to exhibit strong dissolution–reprecipitation processes, which have been intensively studied in the formation of mineral crystals by

hydrothermal fluids, and a large number of well-formed natural minerals were probably generated in some kind of hydrothermal fluid.

The purpose of the present study is to investigate the effect of SCW on the phase and structural properties of an Al_2O_3 supported MnO_2–CuO-containing catalyst (Carulite 300®). The catalyst was used in the oxidative decomposition of ethyl acetate which was used as a model compound. The reaction results are compared to non-catalysed runs. The solid state properties of fresh and used catalyst specimens, like phase composition, bulk and surface composition, particle size, oxidation state and BET surface area, were determined by the usual methods and should give evidence of catalyst alteration.

Experimental

Catalyst

Commercially available Carulite 300® (Carus Chemicals, Inc.) was used as catalyst. The active ingredients were nominally 40–60% MnO_2 and 1–3% CuO, supported on X-ray amorphous Al_2O_3. After the original catalyst pellets were ground, a fraction of 0.3–0.5 mm was sieved and refluxed with water to separate dust particles. After this procedure, the catalyst was dried at 393 K in air for 12 hours.

Catalytic runs

The heterogeneously catalysed experiments were carried in a high-pressure set-up (T_{max} = 673 K, p_{max} = 300 bar) that contains an electrically heated tubular flow reactor (i.d. 0.515 cm, length 35 cm). In addition, non-catalysed runs were carried out in the same set-up. An aqueous solution of the reactant was fed into the apparatus using a HPLC pump (piston pump 305, Gilson). Synthetic air (20.5 vol.% of O_2) was compressed and dosed by a mass flow controller (F-131M, Bronkhorst HITEC). Both the streams were individually heated and mixed at a junction at the entrance of the reactor (Fig. 1). Temperature registration was realized by a thermocouple placed in the feed stream between the mixing junction and the reactor entrance and the temperature of this thermocouple is reported as reaction temperature in this study. The catalyst bed (if used in catalytic runs) was layered on a sintered metal disk at half of the reactor height. After passing the reaction zone, the outlet stream was cooled in a counter-current heat exchanger and depressurised in two steps. The outlet stream was separated into gaseous and liquid phases at ambient conditions. The gaseous product stream was analysed by an on line-GC (GC-14B, Shimadzu) equipped with a thermal conductivity detector (TCD) using a combination of two packed columns (Molecular sieve 13X, 3 m by 0.75 mm i.d.; Porapak N, 1 m by 0.75 mm i.d.). Liquid samples were analysed by an off line-GC (GC-17A, Shimadzu) equipped with an autosampler (AOC-20, Shimadzu) and TCD using a capillary column (FFAP, 30 m by 0.32 mm).

Experiments were carried out in the subcritical (T = 633 K, p = 200 bar, ρ = 0.55 g cm^{-3}) and supercritical regions (T = 673 K, p = 240 bar, ρ = 0.15 g cm^{-3}). Ethyl acetate (Fluka, 99.9%) was fed as an aqueous solution with concentrations always set to 0.02 mol l^{-1}; air was used as oxidant. A molar ratio of ethyl acetate : air : water = 1 : 10 : 2800 was applied, total flow rates were varied from 1–20 ml min^{-1} and the catalyst mass was set to 1 g (fixed bed volume 1 cm^3). Catalyst samples were removed from the reactor for further characterisation after different reaction times (7 h, 21 h, 63 h, 110 h, 175 h, 200 h).

Conversion was calculated as the ratio of reacted moles of organic compound relative to the reactant concentration in the feed. Selectivities were defined as moles of formed product divided by moles of reacted compound, multiplied by the carbon number of the product and divided by that of the reactant, to get stoichiometric corrected values.

Catalyst characterisation

The X-ray powder diffraction (XRD) measurements were carried out using a STADI P (STOE) set-up (Debye–Scherrer geometry, Ge primary monochromator, Cu-Kα_1). The XRD patterns were scanned in the 2Θ range of 5–60° (step width: 0.5°, 100 s per step) and were recorded with a STOE position sensitive detector (PSD). Data interpretation was carried out using the software X-POW (STOE) and the database of Powder Diffraction Files (PDF) of the International Centre for Diffraction Data (ICDD).

The surface analytical studies were performed by an ESCALAB 220iXL spectrometer (Fisons Instruments), consisting of two vacuum chambers: the analyser and a fast entry air lock/preparation chamber. The powdered samples were fixed on a carbon tape (carbon conductive tape, Pelco International) at the top of the sample holder and transferred into the ultra-high vacuum. Monochromatic Al-Kα radiation (1486.6 eV) was applied as the X-ray source with an input power of 300 W. The emerging charge of the sample was equalised with the installed charge compensation. The final peak position was determined using the C1s peak (shifted to 284.5 eV) corresponding to absorbed carbon species. The X-ray photoelectron spectroscopic measurements (XPS) were performed at a constant pass energy of 25 eV. The ESCALAB was

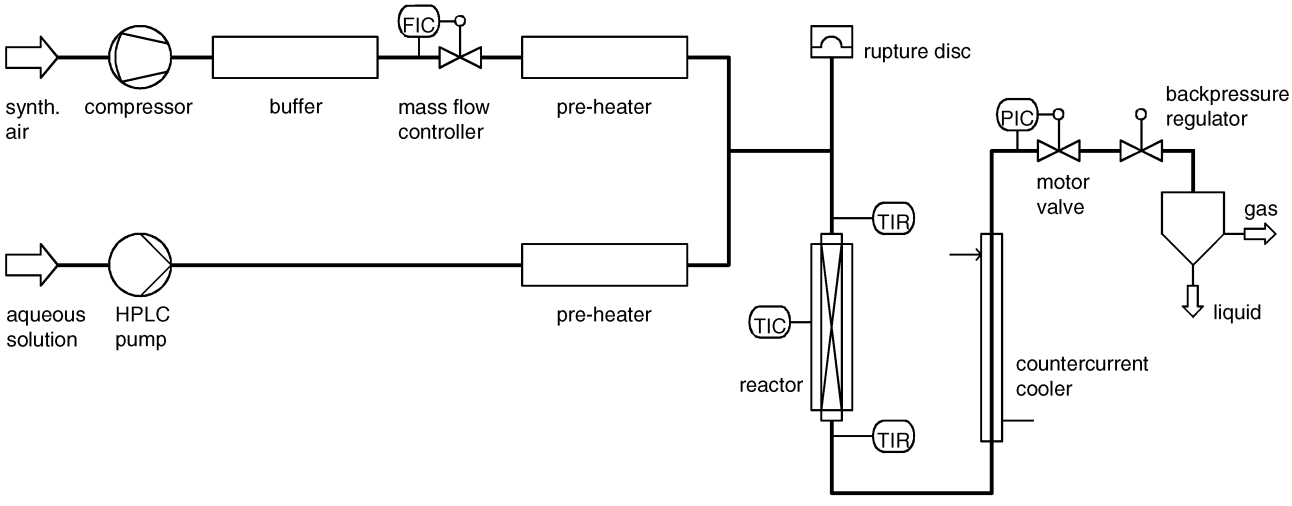

Fig. 1 Scheme of the high-pressure reactor set up.

routinely calibrated with the appropriate XPS lines of Au, Ag and Cu.[29] After background correction[30] the XPS spectra were described and the correct peak positions were determined by Gaussian–Lorentzian peaks if necessary with a tail function to take care of the asymmetry of the XPS signal of transition elements.[31] 95% of the photoelectrons stem from a depth of 6 nm estimated by a realistic mean free path of electrons in the solid state.

The chemical bulk compositions of fresh and used samples were determined by ICP-OES (Optima 3000XL, Perkin-Elmer).

For determination of the morphology and phase distribution of the parent and used catalysts a CM20 (Philips) transmission electron microscope (TEM) with an energy dispersive X-ray analysis (EDX) was used at 200 kV (EDAX, PV9900). The samples were mounted without pretreatment on Lacey-carbon coated copper grids. For localising the copper containing phase in some cases nickel grids were used.

Catalyst surface area was determined by N_2-adsorption according to the BET method at 77 K (Gemini III 2375, Micromeritics). The samples were pretreated at 423–473 K for 1 h under vacuum.

Results and discussion

Heterogeneously catalysed and non-catalysed ethyl acetate conversion

Fig. 2 depicts a comparison of conversion *vs.* residence time of non-catalysed and heterogeneously catalysed ethyl acetate destruction runs under subcritical and supercritical reaction conditions. The results clearly show that the conversion is significantly increased by changing the reaction conditions from a subcritical two-phase reaction mixture to a homogeneous supercritical fluid processing; however, the rate of the hydrolysis of the ester bond seems to be rather unaffected by running the reaction in the presence of a catalyst.

In contrast, the selectivities of the primary reaction products ethanol and acetic acid reveal quite different behaviour with respect to the use of a heterogeneous catalyst. Both the hydrolysis products act in catalysed runs as intermediates in total oxidation to carbon dioxide, but it could not be completely excluded that non-catalysed runs could also lead to oxidative conversion, especially at high residence times. Table 1 shows conversion and selectivity data obtained under subcritical reaction conditions (T = 633 K, p = 200 bar) revealing similar ethanol as well and acetic acid selectivities between *ca.* 35 and 50% for non-catalysed runs. In contrast, the data obtained for heterogeneously catalysed runs clearly demonstrate a significantly decreased selectivity. Moreover, it seems that at short residence times (up to 5 s) in non-catalysed runs both the hydrolysis products are oxidatively converted to a small extent as may be suggested by the slightly increasing selectivity in this time region that could be a hint in this direction. This observation is supported by the results of the supercritical runs (T = 673 K, p = 240 bar) as demonstrated in Table 2 showing similar increases in the selectivities of ethanol and acetic acid at residence times between 0.5 and 2 s. Otherwise nothing particular could be seen in comparison to subcritical runs.

Unfortunately, further kinetic interpretation of the data is much more complicated and would need further investigation with respect to analytical errors due to the small quantities of the reactant and products.[26] Furthermore, additional analysis is required for complete determination of carbon dioxide in the liquid phase. Then a power-law rate equation could be calculated if such data were obtained but, in general, up to now available kinetics information for catalytic reaction in the compressed water phase is still limited, with some exceptions.[21,27]

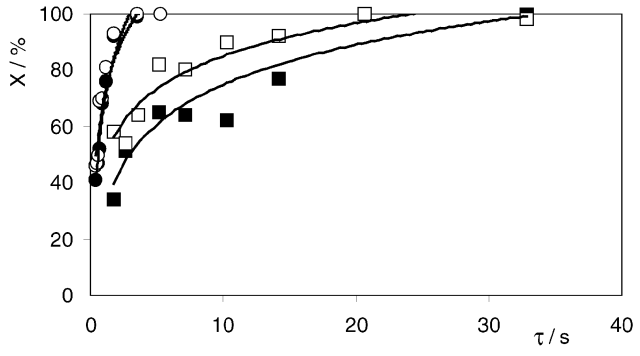

Fig. 2 Ethyl acetate conversion *vs.* residence time during subcritical reaction processing (200 bar, 633 K, ethyl acetate : oxygen : water = 1 : 10 : 2800; ■ non-catalysed, □ heterogeneously catalysed) and supercritical reaction processing (240 bar, 673 K, ethyl acetate : oxygen : water = 1 : 10 : 2800; ● non-catalysed, ○ heterogeneously catalysed).

Table 1 Survey of ethyl acetate conversion (X), and ethanol and acetic acid selectivity (S(EtOH), S(HAc)) in non-catalysed and heterogeneously catalysed runs under subcritical reaction conditions (T = 633 K, p = 200 bar, molar ratio of ethyl acetate : oxygen : water = 1 : 10 : 2800)

Conditions	τ/s[a]	X (%)	S(EtOH) (%)	S(HAc) (%)
Non-catalysed runs	1.8	34	38	27
	3.6	64	46	34
	5.2	65	53	43
	7.1	64	33	34
	10.3	62	39	31
	20.6	100	32	34
	32.9	100	33	41
Heterogeneously catalysed runs	1.8	58	7	1
	3.6	64	14	4
	5.2	82	14	4
	7.1	80	11	4
	10.3	90	12	8
	20.6	100	2	0
	32.9	98	8	4

[a]Related to the overall volume of the fixed bed (fixed bed volume = 1 cm^3).

Table 2 Survey of ethyl acetate conversion (X), and ethanol and acetic acid selectivity (S(EtOH), S(HAc)) in non-catalysed and heterogeneously catalysed runs under supercritical reaction conditions (T = 673 K, p = 240 bar, molar ratio of ethyl acetate : oxygen : water = 1 : 10 : 2800)

Conditions	τ/s[a]	X (%)	S(EtOH) (%)	S(HAc) (%)
Non-catalysed runs	0.44	41	26	21
	0.52	48	29	27
	0.60	47	33	27
	0.72	52	38	26
	1.18	76	39	34
	1.78	92	48	45
	3.56	99	47	39
Heterogeneously catalysed runs	0.44	46	18	5
	0.52	47	20	3
	0.60	50	26	10
	0.72	69	16	6
	1.18	81	27	1
	1.78	93	24	10
	3.56	100	21	7

[a]Related to the overall volume of the fixed bed (fixed bed volume = 1 cm^3).

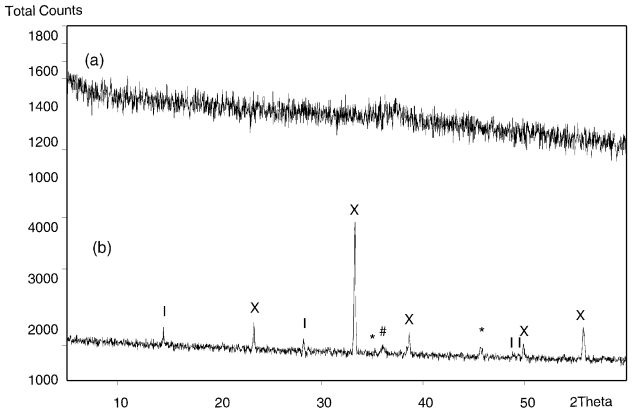

Fig. 3 XRD patterns of parent Carulite 300® (a) and spent catalyst exposed to sub- and supercritical operation for 200 h on-stream (b) (I = OH); X = Mn_2O_3; * = Al_2O_3; # = $CuMn_2O_4$, $Cu_{1.5}Mn_{1.5}O_4$, Mn_2O_3, Mn_3O_4).

Phase analysis

Fig. 3 depicts XRD patterns of the parent material and a used catalyst sample that was exposed to sub- and supercritical reaction conditions for 200 h. The fresh catalyst (pattern (a)) is an almost complete X-ray amorphous material with no indication of the existence of metal oxide phases (MnO_x, CuO_x, Al_2O_3). In contrast, the spent catalyst (pattern (b)) reveals a totally changed XRD pattern. The sample shows highly crystalline components with Mn_2O_3 and AlO(OH) as the main phases, and the BET surface areas of these samples are decreased by *ca.* 95% (fresh sample: 264 $m^2\ g^{-1}$, used sample: 15 $m^2\ g^{-1}$). Interestingly, all reflections of the Mn_2O_3 phase show a slight difference to the values of the PDF card 78-390. The refinement of the cubic lattice constant of Mn_2O_3 (9.43 Å) led to a new declined value of 9.31 Å. Beside these main phases, there are small indications of the existence of Al_2O_3 and some mixed-oxide $CuMnO_x$ phases (*e.g.* $CuMn_2O_4$, $Cu_{1.5}Mn_{1.5}O_4$) that seem to be superimposed by other Mn-oxides resulting in the rather broad reflection at $2\Theta = 35.28$.

For further catalyst characterisation, some catalyst specimens were chosen that were exposed to the reaction conditions for different times (7 h, 21 h, 63 h, 175 h) to gain more insight into structural alterations occurring on-stream (Fig. 4). The XRD pattern of the catalyst after 7 h on-stream (pattern (a)) shows some weak reflections that point to crystalline proportions in contrast to the parent solid. These reflections can be indexed as Mn_3O_4, mainly. Beside Mn_3O_4, some hints for the existence of mixed-oxide phases such as $MnAl_2O_4$ (galaxite) or Mn_2AlO_4 with identical crystal system and lattice constants and probably $Cu_{1.5}Al_{1.5}MnO_4$ were found. Increasing the reaction time up to 21 h leads to no significant changes in the phase composition but the crystallinity of the sample is further increased as can be clearly seen from the reflection intensity of pattern (b). A more drastic alteration can be observed evaluating the pattern (c) of the catalyst sample removed from the reactor after 63 h on-stream. The crystallinity is increased again but the former well-shaped Mn_3O_4 reflections are almost vanished, only a weak reflection of mixed Mn–Cu-oxides still remains. Instead, well crystalline Mn_2O_3 is formed and AlO(OH) could be identified as crystalline phase generated from Al_2O_3 by hydrolysis. Pattern (d) of the sample obtained after 175 h on-stream does not show further significant alterations; only the main reflection of mixed Mn–Cu-oxides has totally vanished. Pattern (d) looks quite similar to that of the 200 h sample (see Fig. 3, pattern (b)). Additionally, there are some changes of the reflection positions for Mn_2O_3 that are shifted to higher values probably due to the shrinking of the unit cell as discussed above. The following conclusions can be drawn from the XRD investigations: (i) the almost X-ray amorphous parent sample is subject to major structural transformation on-stream, *i.e.* dissolution–reprecipitation and crystallisation processes due to SCW conditions, (ii) mainly Mn_2O_3 is formed as the stable crystalline phase from bulk MnO_2 by reduction and (iii) the Al_2O_3 support transformation into AlO(OH) is effected by hydrolysis.

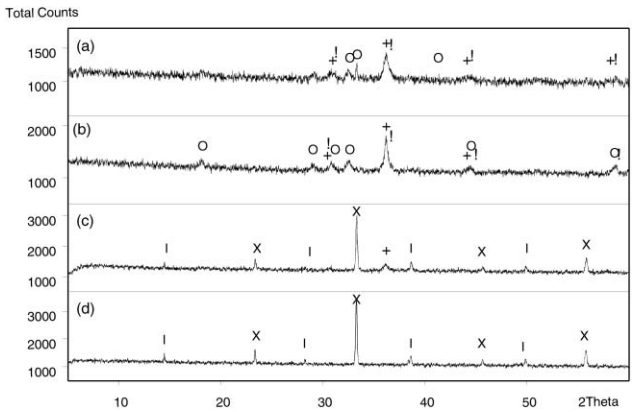

Fig. 4 XRD patterns of spent catalysts removed from the reactor after 7 h (a), 21 h (b), 63 h (c) and 175 h (d) (+ = $Cu_{1.5}Mn_{1.5}O_4$, ! = $MnAl_2O_4$, O = Mn_3O_4, I = AlO(OH), X = Mn_2O_3).

Bulk and surface composition

The bulk proportions of Mn, Cu and Al as determined by ICP-OES are summarised in Table 3. The most significant result is the drastic increase of the amount of these components already after 7 h on-stream. This increase might be explained by a loss of oxygen at the very beginning of catalyst exposure to SCW conditions assuming that the most part of the non-analysed remainder is oxygen and/or hydroxide. This oxygen loss seems to be due to reduction of transition metal oxides, as is proven by the observed generation of crystalline Mn_3O_4 by XRD, otherwise, reduced specimens could exist as X-ray amorphous phases at this stage. However, such tremendous changes were only observed investigating the first spent sample, analyses of other catalysts removed from the reactor after increased time-on-stream revealed no further significant changes.

The surface composition as measured by XPS differs from the bulk composition. Table 4 demonstrates these differences and the dramatic changes observed on-stream. Aluminium is the main cationic component on the surface of the parent sample in contrast to the bulk where Mn shows the largest proportion. The surface composition significantly alters up to 21 h. The amounts of both manganese and copper increased in

Table 3 Mn, Cu and Al bulk composition changes with time-on-stream (TOS)

TOS/h	Mn/atom%	Cu/atom%	Al/atom%
0 (parent)	16.7	3.2	6.4
7	25.3	4.9	9.8
21	25.3	4.9	9.8
63	25.0	4.5	9.1
110	25.5	4.9	9.6

Table 4 Surface composition of parent and catalytically tested Carulite 300® samples, determined by XPS, relative to time-on-stream (TOS)

TOS/h	Mn/atom%	Cu/atom%	Al/atom%	O/atom%	C/atom%
0 (parent)	8.0	3.9	16.3	63.8	7.6
7	9.0	2.4	7.1	47.0	34.6
21	17.0	12.8	9.2	45.4	15.6
63	11.4	14.8	12.4	46.3	15.2
110	11.0	11.5	13.7	53.2	10.6

this period whereas the proportion of aluminium declined with a slight minimum at 7 h on-stream. Only small alterations could be observed after 21 h on-stream. A possible explanation for such drastic changes in the surface composition especially in the beginning of the reaction might be seen in a dramatic alteration of the outer particle surface including particle size and composition due to the mentioned dissolution–reprecipitation processes. Decreasing oxygen content at the surface was observed similar to the bulk properties. At the beginning of the reaction considerable carbon deposits could be detected on the surface (after 7 h). This might be explained by the drastic alterations in phase behaviour, probably leading to fixation as well as adsorption of reactant and/or product molecules. Progressive crystallisation and surface reconstruction of the catalyst seem to prevent further deposition of carbonaceous compounds.

Fig. 5 depicts typical XPS spectra of the Cu 2p (a), Mn 2p (b) and Mn 3s (c) regions of parent and used samples. Only bivalent Cu is found in the spectrum of the parent sample, showing the typical satellites. An additional shoulder at lower binding energies is observed for the samples removed from the reactor after different reaction times. The origin of this shoulder could be assigned to Cu reduced during the reaction that interacts strongly with other surface compounds, may be MnO_x phases. However, it is not possible to distinguish between Cu(I) and Cu(0) because the Cu LMM Auger peaks were too small to get Auger parameters which would be necessary for definite assignment to one of these oxidation states.

Differentiation of Mn(III) and Mn(IV) oxidation states can be done only by evaluation of the width of the splitting of the Mn 3s peak. The reason for this rather complicated procedure is the small difference in binding energy of the Mn 2p and 3p electrons representing Mn(III) and Mn(IV) oxidation states. Fig. 6 shows the obtained width of the splitting Δ (3s) *vs.* time-on-stream. It is clearly shown that almost all surface Mn(IV) of the parent sample is reduced to Mn(III) after 7 h on-stream. Further processing increases the reduction degree of surface Mn which tends to favour the formation of the mixed-valent oxide Mn_3O_4. This seems to be somewhat in contrast to the XRD observations that indicate Mn_2O_3 as the most stable crystalline phase after *ca.* 60 h, but we should again note here the difference between the bulk XRD method characterising crystalline parts of the whole solid and the XPS method analysing the first layers of the surface. The formation of MnO could not be observed. This is also unlikely as there is still a certain amount of oxygen in the system leading to the formation of a medium valence state between Mn(II) and Mn(III).

Furthermore, aluminium does not show any change of electronic state during the whole reaction time.

Morphology

The parent sample consists of small particles in the size range 5 to 20 nm (Fig. 7). In some cases the lattice planes fit the (110) and (200) planes of the tetragonal α-MnO_2. An overall Mn : Al ratio of 60 : 40 was found for the agglomerates with EDX analysis results that agree quite well with the ICP data.

After short reaction time (7 h) the morphology changes completely. Square-like particles arise that only contain Mn and Cu. Additionally, two different Al-containing phases in the

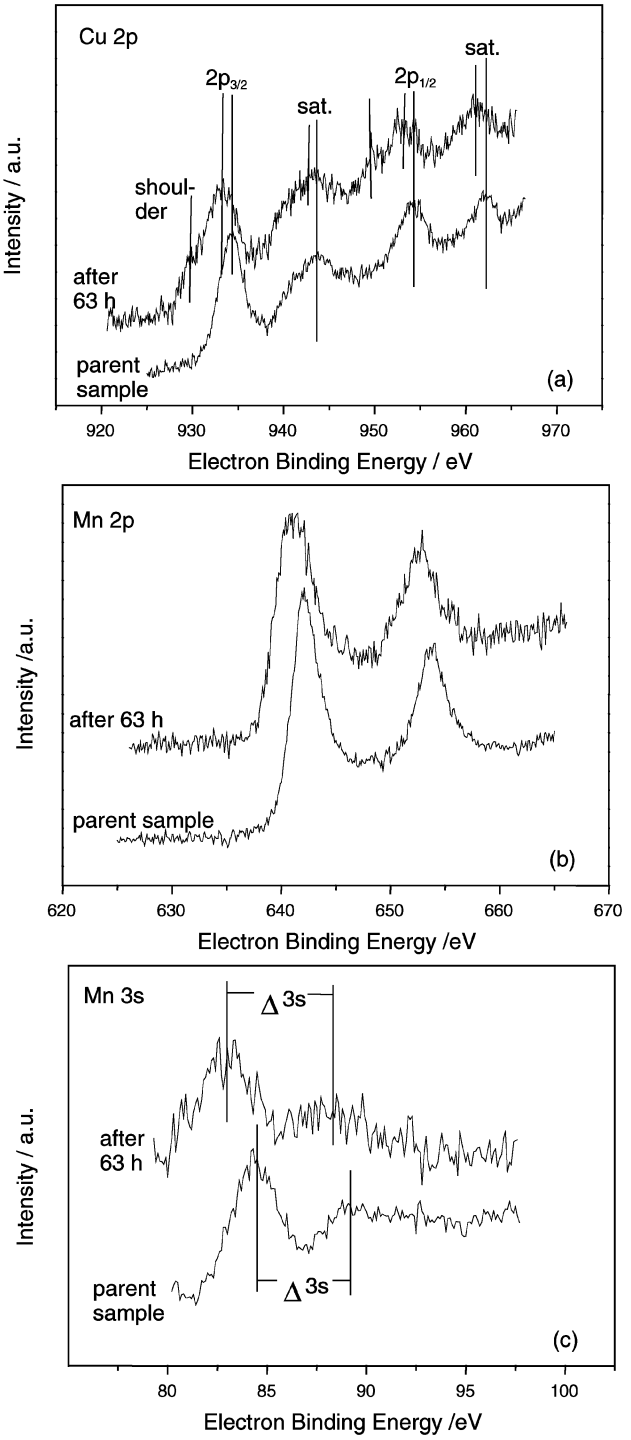

Fig. 5 Typical XPS spectra of the Cu 2p (a), Mn 2p (b) and Mn 3s (c) regions of the parent sample and of the catalyst removed from the reactor after 63 h.

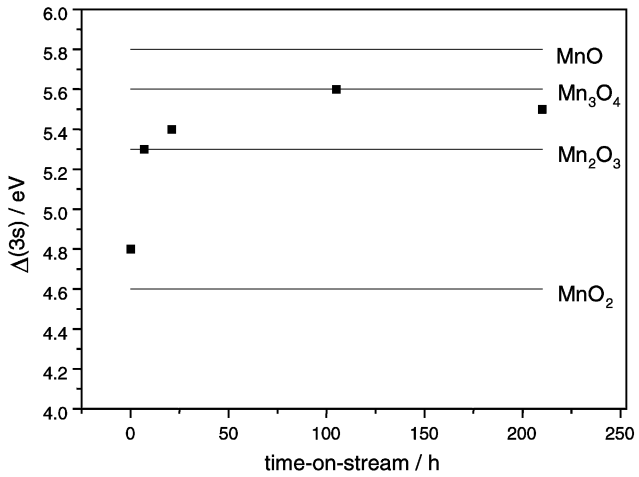

Fig. 6 Splitting of the Mn 3s peak Δ(3s) observed in XPS spectra of the catalysts *vs.* time-on-stream. The reference values for the different MnO_x are shown.

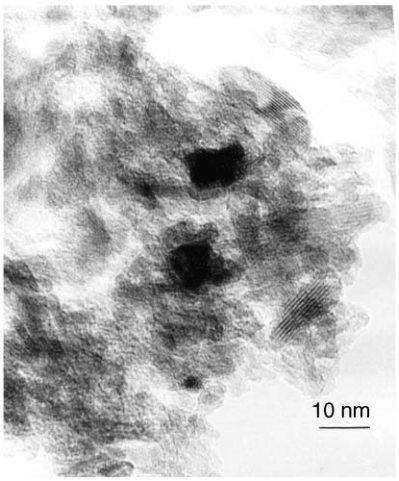

Fig. 7 TEM micrograph of the parent sample.

shape of squares and needles appear (Fig. 8a). In both these phases no copper was detectable. An Al : Mn ratio of 2 : 1 for the squares was found by EDX, which would agree very well with the galaxite ($MnAl_2O_4$) phase observed by XRD. The second, needle-like crystalline phase contains an Al : Mn ratio of 1 : 1. However, no appropriate crystalline phase could be detected by XRD; moreover, the data base used for XRD contains no files related to a copper-free structure with Al : Mn in a ratio of 1 : 1. Maybe, the co-existence of identical $MnAl_2O_4$ and Mn_2AlO_4 lattices in one needle could explain such a result. Furthermore, no hint could be found pointing to copper-containing Al,Mn-phases like $Cu_{1,5}Al_{1,5}MnO_4$ as observed by XRD.

After 21 h on-stream the needles disappeared but the same phases as mentioned above were found: manganese in connection with copper (particle size about 100 nm), 20–50 nm particles with Al : Mn = 1 : 1 and a galaxite phase that grew up to 200 nm; the latter two particles are shown in Fig. 8b. After a reaction time of 63 h further significant changes were observed (Fig. 8c). Mn,Cu-containing polycrystalline flat plates up to a diameter of 2 μm are detectable. Furthermore, EDX analysis reveal that the copper was still connected with manganese whereas XRD reveals an increasing amount of pure manganese oxides and no evidence for any new copper-rich phase. The XPS data showing a significant increase of copper at the surface at reaction times of more than 21 h and XRD observations of vanishing Cu,Mn-oxides lead to the conclusion that copper seems to be concentrated at the surface of the manganese oxides. Secondly, needles longer than 3 μm with a thickness of 100 nm were found and can be related to AlO(OH) as also observed by XRD.

The final state after 200 h reaction time shows the same features (Fig. 8d), but the manganese oxide phases changed from polycrystalline plates to compact, well-crystallized particles with sizes up to 1 μm.

Conclusions

Summarising the results, the investigations have shown that ethyl acetate can be exclusively converted to ethanol and acetic acid in sub- and supercritical water using a continuous high-pressure set-up. The reaction runs faster in the supercritical region in comparison to processing under sub-critical conditions that needs approximately threefold higher residence times. The application of a heterogeneous catalyst (MnO_2, CuO on Al_2O_3; Carulite 300®) tested in sub- and supercritical water regions has no significant influence on conversion but distinct changes in reaction selectivity were observed, *i.e.* ethanol as well as acetic acid were consecutively converted to carbon oxides. The catalyst underwent profound alteration during exposure in sub- and supercritical water due to strong hydrothermal conditions that lead to deep dissolution–reprecipitation processes. However, no significant changes in either catalyst activity or reaction selectivity were observed over a period of 200 h. The effect of hydrothermal conditions on the solid catalyst could be enlightened by various characterisation techniques. XRD showed the formation of several crystalline catalyst proportions with increasing time-on-stream. Finally, crystalline Mn_2O_3 and AlO(OH) seem to be the stable catalyst phases. ICP and XPS revealed on the one hand tremendous changes in bulk and surface composition due to reduction of Mn(IV) to Mn(III) and Cu(II) to Cu(I) and/or Cu(0), probably, but otherwise, phase transformations may also lead to new surface compositions. No significant hints for catalyst component leaching were found. TEM investigations impressively demonstrated morphology alterations, changes in crystal composition and crystal growth with time-on-stream. Taking the characterisation results into account, Mn(III) oxide

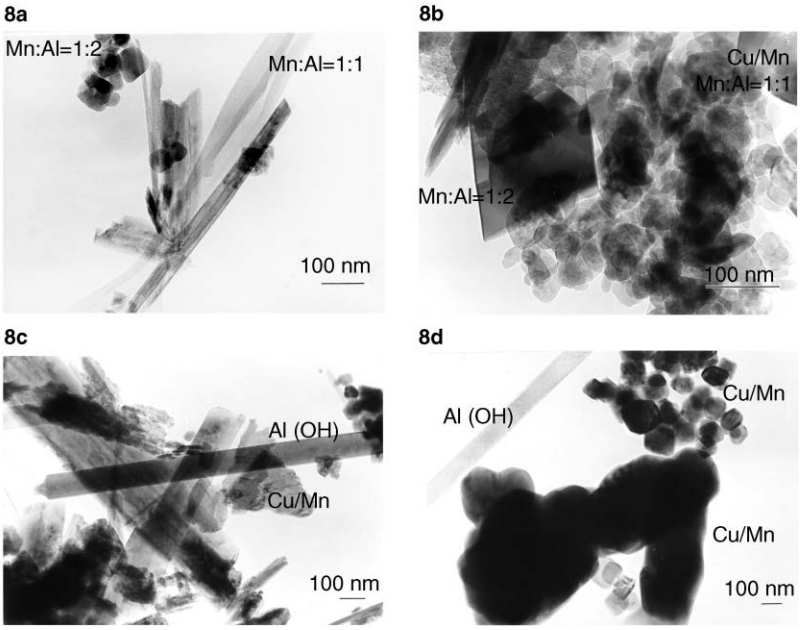

Fig. 8 TEM micrographs of used catalyst samples after (a) 7h, (b) 21 h, (c) 63 h and (d) 200 h on-stream.

containing phases might be responsible for oxidative conversion of the hydrolysis products to carbon oxides.

Acknowledgement

The authors thank Mr. A. Krepel and Mrs. W. Winkler for experimental assistance and Nirmal Singh of Carus Chemical, Inc. for transferring catalyst samples. The financial support of the Federal Ministry of Education and Research, Germany and the Senate of Berlin is acknowledged (Project No. 03 C3012 0).

References

1 P. W. Atkins, *Physical Chemistry*, 3rd edition, Oxford University Press, 1986, p. 663.
2 R. W. Shaw, T. B. Brill, A. A. Clifford, C. A. Eckert and E. U. Franck, *Chem. Eng. News*, 1991, **69**, 26.
3 D. Bröll, A. Krämer, M. Jung, C. Kaul, P. Krammer, T. Richter, H. Vogel and P. Zehner, *Angew. Chem.*, 1999, **111**, 3180.
4 M. Siskin and A. R. Katritzky, *Chem. Rev.*, 2001, **101**, 825.
5 A. R. Katritzky, D. A. Nichols, M. Siskin, R. Murugan and M. Balasubramanian, *Chem. Rev.*, 2001, **101**, 837.
6 J. Jung and M. Perrut, *J. Supercrit. Fluids*, 2001, **20**, 179.
7 E. U. Franck, *Ber. Bunsen-Ges. Phys. Chem.*, 1984, **88**, 820.
8 J. F. Connolly, *J. Chem. Eng. Data*, 1966, **11**, 13.
9 P. E. Savage, *Chem. Rev.*, 1999, **99**, 603.
10 Y. Ikushima, K. Hatakeda, O. Sato, T. Yokoyama and M. Arai, *Angew. Chem., Int. Ed.*, 1999, **38**, 2910.
11 E. F. Gloyna, L. Li and R. N. McBrayer, *Water Sci. Technol.*, 1994, **30**, 1.
12 P. E. Savage, S. Gopalan, T. I. Mizan, C. J. Martino and E. E. Brock, *AIChE J.*, 1995, **41**, 1723.
13 C. Kaul, H. Vogel and H. E. Exner, *Materialwiss. Werkstofftech.*, 1998, **30**, 326.
14 J. Yu and P. E. Savage, *Appl. Catal. B: Environ.*, 2001, **31**, 123.
15 J. Yu and P. E. Savage, *Ind. Eng. Chem. Res.*, 1999, **38**, 3793.
16 J. Yu and P. E. Savage, *Ind. Eng. Chem. Res.*, 2000, **39**, 4014.
17 Y. Oshima, K. Tomita and S. Koda, *Ind. Eng. Chem. Res.*, 1999, **38**, 4183.
18 K. C. Chang, L. Li and E. F. Gloyna, *J. Hazard. Mater.*, 1993, **33**, 51.
19 M. Krajnc and J. Levec, *Appl. Catal. B: Environ.*, 1997, **13**, 93.
20 M. Krajnc and J. Levec, *Appl. Catal. B: Environ.*, 1994, **3**, L101.
21 Z. Y. Ding, S. N. V. K. Aki and M. A. Abraham, *Environ. Sci. Technol.*, 1995, **29**, 2748.
22 M. A. Frisch, M.S. Thesis, University of Texas, Austin, 1992.
23 M. A. Frisch, Ph.D. Thesis, University of Texas, Austin, 1995.
24 S. N. V. K. Aki and M. A. Abraham, *Ind. Eng. Chem. Res.*, 1999, **38**, 358.
25 X. Zhang and P. E. Savage, *Catal. Today*, 1998, **40**, 333.
26 U. Armbruster, A. Martin and A. Krepel, *Appl. Catal. B: Environ.*, 2001, **31**, 263.
27 P. E. Savage, *Catal. Today*, 2000, **62**, 167.
28 P. G. Jessop and W. Leitner, *Chemical Synthesis Using Supercritical Fluids*, Wiley-VCH, Weinheim, 1999.
29 M. T. Anthony and M. P. Seah, *Surf. Interface Anal.*, 1984, **6**, 95.
30 D. A. Shirley, *Phys. Rev. B*, 1972, **5**, 4709.
31 R. O. Ansell, T. Dickinson, A. F. Povey and P. A. M. Sherwood, *J. Electroanal. Chem.*, 1979, **98**, 79.